Chronic Pb^{2+} exposure causes theta-band hypersynchrony disrupting sensory motor gating and exacerbating absence seizures

Abbreviated Title: LEAD EXPOSURE CAUSES HIPPOCAMPAL HYPERSYNCHRONY

Nathan W. Schultheiss[1], Jennifer L. McGlothan[2], Tomás R. Guilarte[2*], Timothy A. Allen[1,2,3*]

[1]Department of Psychology, Florida International University, Miami, FL, 33199
[2]Department of Environmental Health Sciences, Robert Stempel College of Public Health, Florida International University, Miami, FL, 33199
[3]Cognitive Neuroscience Program, Florida International University, Miami, FL, 33199

Number of figures: 4
Number of supplemental figures: 6
Number of tables: 1
Number of text pages: 40

*Corresponding Authors:

Timothy A. Allen, PhD
Department of Psychology
email: tallen@fiu.edu
Website: http://allenlab.fiu.edu/
Twitter: @AllenNeuroLab

Tomás R. Guilarte, PhD
Department of Environmental Health Sciences
email: tguilart@fiu.edu
website: https://stempel.fiu.edu/brain-behavior-environment-laboratory/
Twitter: @guilartelab

Address:
Florida International University
11200 SW 8th Street
Miami, FL, 33199

Conflict of Interest: The authors declare no competing financial interests.
Acknowledgements: This work was supported by R01 ES006189 to T.R.G. and R01 MH113626 to T.A.A.
Keywords: hippocampus, schizophrenia, lead neurotoxicity, pre-pulse inhibition

ABSTRACT

Chronic lead (Pb^{2+}) exposure from childhood contributes to an array of cognitive and behavioral dysfunctions including impaired attention and intellectual ability, learning and memory deficits, and delinquency. It is also an environmental risk factor for adult psychopathologies, most notably schizophrenia and epilepsy. Pb^{2+} is a potent N-methyl-D-aspartate receptor (NMDAR) antagonist and exposure during early life elicits a cascade of cellular neurotoxic effects that alter the developmental trajectory leading to a loss of parvalbumin-expressing interneurons in hippocampus and altered synaptic transmission. Little is known, however, about the impact of chronic Pb^{2+} exposure on hippocampal network dynamics which serve as a link between cellular-molecular effects and cognitive-behavioral consequences of Pb^{2+} neurotoxicity. Here, we tested the effects of chronic Pb^{2+} exposure on the hippocampal local field potential (LFP) of freely-behaving rats. Pb^{2+} exposure caused striking theta rhythmic hypersynchrony and heightened behavioral modulation of theta during locomotor behavior. Pb^{2+} exposure also markedly exacerbated absence seizures appearing in the LFP as spike-wave discharges with a theta-band fundamental frequency and strong theta-harmonic synchronization. Mechanisms of theta rhythmogenesis have been implicated in impairments of prepulse inhibition of the acoustic startle reflex (PPI), so we tested the effect of Pb^{2+} exposure on PPI in male and female rats at different developmental timepoints. We found that adult males (PN50 and 120), but neither females nor juvenile males showed reduced PPI independent of changes in the startle reflex. This pattern recapitulates sex- and age-dependencies of PPI disruption in schizophrenic patients. Overall, these results are consistent with the hypothesis that Pb^{2+} is an environmental risk factor for psychopathology in adulthood, especially those symptoms related to cognitive and sensory-motor gating processes that depend on rhythmic coordination of network activity in the hippocampus.

Introduction

Environmental exposure to lead (Pb^{2+}) is a major health problem affecting millions of people worldwide. Pb^{2+} exposure in children has been linked to reduced intellectual abilities, increases in delinquent and antisocial behaviors, and attention deficit and hyperactivity disorder (Needleman et al., 2002; 2004; Miranda et al., 2007; Canfield et al., 2003; Caito & Aschner, 2017). Further, early life Pb^{2+} exposure has been proposed as an environmental risk factor for adult psychopathology, within significant comorbidity with both epilepsy and schizophrenia (Opler et al., 2004; 2008). A current leading hypothesis is that schizophrenia is best understood as the result of interactions between genetic and environmental factors (Guilarte et al., 2012), with evidence that Pb^{2+} exposure exacerbates cognitive and behavioral deficits in the DISC1 knock out mouse model of schizophrenia (Abazyan et al., 2014).

Understanding the relationship between Pb^{2+}-exposure and mental health pathologies requires a neurobiological approach to establishing the link between genetic and environmental factors. At the cellular and molecular levels, much is known about Pb^{2+} effects on the developing brain. Pb^{2+} is a potent N-methyl-D-aspartate (NMDA) receptor antagonist (Guilarte, 1997; Guilarte & Miceli, 1993; Guilarte & Miceli, 1992). Low-to-moderate Pb^{2+} levels in the brain (which has no endogenous function) leads to NMDAR hypoactivity, which can alter the developmental trajectory of the NMDAR subunits (Guilarte & McGlothan, 1998; Nihei et al., 2000), and impair the maintenance synaptic long-term potentiation (Nihei et al., 2000). At the cellular level, Pb^{2+} exposure causes a reduction in the number of parvalbumin-labeled GABAergic interneurons in the hippocampus and agranular medial prefrontal cortex (Stansfield et al., 2015), a hallmark cellular pathology in schizophrenic brains (e.g., Hashimoto et al., 2003). At the level of the whole brain, annual childhood blood Pb^{2+} levels have been found to be inversely correlated with cortical gray matter volume (Brubaker et al., 2010). Likewise, an electroencephalography (EEG) study of Pb^{2+}-exposure, as measured by tooth Pb^{2+}, showed there are significant alterations in delta, theta and gamma bands

related to cognitive function, the severity of which corresponded to the exposure levels (Needleman, 1983).

However, the bridge between the cellular-molecular and cognitive-behavioral levels is not well understood. Linking these levels requires animal models of Pb^{2+} exposure allowing for invasive techniques that can establish a causal link between Pb^{2+} exposure, specific neurobiological mechanisms, and behaviorally-relevant network consequences. Here, we performed chronic *in vivo* hippocampal recordings from a well-established rodent model of Pb^{2+} exposure during open field behaviors (Schultheiss et al., 2020). This initial study of the rhythmic network effects of chronic Pb^{2+} exposure focused on the hippocampus because chronic Pb^{2+}-exposure causes reliable and severe deficits in hippocampal-dependent spatial learning (Kuhlmann et al., 1997; Jett et al., 199; Munoz et al., 1988) which can be ameliorated with environment enrichment (Cao et al., 2008; Guilarte et al., 2002), similar to other hippocampal insults. Likewise, Pb^{2+}-exposure causes contextual but not cued fear conditioning deficits (Jaako-Movits et al., 2005; McGlothan et al., 2008; Wang et al., 2016), in addition to fear extinction impairments (McGlothan et al., 2008). These behavioral results are consistent with the central role of hippocampal networks in mediating the effects of chronic Pb^{2+}-exposure in psychotic disorders.

Our recordings and analysis focused on the spectral content of local field potentials (LFPs) from the hippocampus in of Pb^{2+}-exposed rats using multisite silicon probes during stationary and running behaviors. LFPs are a good choice to examine network properties because they reflect the rhythmic synchrony among neurons aggregating local and long-range synaptic potentials. We observed several key abnormalities, most notably excessive hypersynchrony of the theta rhythm and increased amplitude of gamma oscillations, elevated behavior-related changes in the theta and gamma bands, and exacerbated intensity and incidence of absence seizures. Hypersynchrony is detrimental to local network processing and has been observed in other disorders. For example, hippocampal hypersynchrony in the theta and slow gamma ranges have also been observed in the

LFP recordings of the freely-behaving *Fmr1-KO* mouse, a genetic model of Fragile X syndrome which is characterized by intellectual disability (Arbab et al., 2018).

Next, because over activation of the hippocampus is known to cause impaired sensory-motor gating (Bast et al., 2001a,b; Bast et al. 2003), we followed the network finding up by looking at the consequences of Pb2+-exposure on prepulse inhibition of the startle reflex (PPI). We found that Pb^{2+}-exposure caused large and reliable sensory-motor gating deficits in male, but not female, adult rats in developmentally-relevant pattern (PN50 and PN120, but not PN28). These effects could not be attributed to baseline startle levels, and are in line with the Pb^{2+} hypothesis of schizophrenia because PPI impairments are a hallmark pathological phenotype in the disease.

Altogether the present findings show that Pb^{2+} exposure leads to pathological theta and gamma hypersynchrony in the hippocampus, increases seizures, and causes sensory-motor gating deficits. These abnormal hippocampal network effects may explain both the cognitive and the sensory-motor gating deficits seen in adult psychopathologies resultant of Pb^{2+} exposure, and suggests normalizing hippocampal network dynamics as a therapeutic strategy.

Methods

Subjects. Nine adult male Long-Evans rats were used in electrophysiological experiments. Five of these were chronically exposed to lead (Pb^{2+}), and four were controls. Two hundred thirty rats were used in PPI experiments. These rats were evenly divided into twelve groups (18-21 per group) corresponding to all combinations of (1) Pb^{2+} exposure and controls, (2) males and females, and (3) three ages at the time of testing. All rats were individually housed in a climate-controlled vivarium on a reversed 12hr light/dark cycle, and experiments were conducted during the dark cycle active periods. Rats had free access to food and water when in their home cages, but no food or rewards were available during behavioral sessions. All studies were carried out in strict accordance with the recommendations in the Guide for the Care and Use of Laboratory Animals of the National Institutes of Health under protocols approved by Florida International University Institutional Animal

Care and Use Committee. Data from the four control rats in the electrophysiological experiments were previously analyzed to establish the relationships of hippocampal spectral modes to behaviors (Schultheiss et al., 2020). The present study focuses on the effects of Pb^{2+} exposure and all analyses presented here are new.

Breeding and Chronic Pb^{2+} Exposure. Prior to breeding, adult female rats (225-250 g) were purchased from Charles River Laboratories and randomly assigned to a Prolab RMH-1000 diet containing 0 (control) or 1500 ppm lead acetate (PbAc) (Dyets, Inc., Bethlehem, PA). After 10-14 days of acclimation to the diet, each dam was paired with a non-exposed adult male Long Evans rat (250-275 g; Charles River Laboratories) to breed over 3 days. Litters were culled to 10 pups on postnatal day one (PN1). Dams were maintained on their respective diet, and at PN21 male pups were weaned onto the same diet and maintained for the duration of the experiments.

Silicon probe implants. All electrophysiological procedures were the same as we have previously described (see Schultheiss et al., 2020 for details). Briefly, silicon probes with 32 recording electrodes arranged as eight tetrodes were surgically implanted for recording local field potentials (LFPs) from dorsal hippocampus (HC). The eight tetrodes were distributed across four shanks of the probe at tip-to-tetrode depths of 78 µm and 228 µm (NeuroNexus A4X2-tet-5mm). Shanks were separated by 200 µm giving each probe a total length of 0.67 cm which was oriented medial-lateral when implanted to sample along the proximal-distal axis of the CA1 subregion of HC. Electrode impedances were 1.23 ± 0.32 MΩ.

Surgical procedures. The rats used in electrophysiological experiments weighed 600-700 g at the time of surgery. General anesthesia was induced with isoflurane (5%) mixed with oxygen (0.8 L/min) that was continuously delivered throughout surgery at 1-4% as needed. Body temperature was monitored throughout surgery, and a Ringer's solution (5% dextrose) was given periodically to maintain hydration (1 ml increments every 60-90 minutes). Once the hair over the scalp was cut, rats were placed in a stereotaxic device, and glycopyrrolate (0.5 mg/kg, s.c.) was administered to assist respiratory stability. Ophthalmic ointment was then applied to the eyes. Four injections of

marcaine were made to the scalp (~0.1 ml, 7.5 mg/ml, s.c.), and a rostrocaudal incision was made exposing the skull. The pitch of the skull was leveled between bregma and lambda, two stainless steel ground screws were placed in the left parietal bone, and five titanium support screws were anchored to the skull. Rectangular craniotomies were drilled to accommodate the probe shanks centered on coordinates A/P -3.24 mm, M/L 2.7 mm. After removal of the dura, the probe was lowered on the stereotaxic arm until the tips of the probe shanks were just above the cortical surface. Then, the ground wire was attached to the ground screws, and implants were lowered further until the electrodes reached a depth of ~2.8 mm below the cortical surface. A thin layer of sodium alginate was applied in the craniotomy to protect the exposed surface of the brain, and dental cement was applied to permanently secure the implant to the skull screws. Neosporin® was applied to the skin surrounding the implant, and flunixin (2.5 mg/kg, s.c.) was given for analgesia. Following surgery, rats were allowed to rest on a heating pad until ambulatory, prior to being returned to their home cages. Neosporin® and flunixin were given again on the day following surgery, and rats were monitored closely for five days to ensure that body weight was maintained. Daily Baytril injections (s.c.) were also given for five days to protect against postsurgical infection. A minimum of one week was reserved for recovery prior to beginning experiments.

Behavioral Setup. All electrophysiological experiments were conducted in a large open field environment (122 x 118 x 47 cm). A custom-made white cutting board served as the floor of the behavioral arena, and the interior walls were lined with white vinyl. The arena was mounted on stilts 72 cm above the floor and the exterior was wrapped in grounded Faraday shielding. Two video cameras were used for behavioral tracking with a bird's eye view. These were mounted 28 cm apart from one another,150 cm above of the arena floor, providing ~4.6 pixel/cm resolution in recorded videos and corresponding tracking data.

The entire behavioral apparatus was enshrouded with black curtains suspended from the ceiling and extending to the floor. Small gaps at the Velcro® closures between the four curtain panels were used to observe rats covertly to monitor that the head-stage, cables, and elastic

tethers were not tangled, and to confirm that rats were awake during periods of relative inactivity. All room lights were kept off during recording sessions, and the white arena was illuminated dimly with red light from LED strips mounted above at the level of the video cameras.

During behavioral sessions rats were placed on the arena floor and recorded without any intervention except for infrequent behavioral checks or to adjust cables or connections.

Electrophysiological recordings. Throughout each experiment wide-band neural data were acquired with a Plexon OmniplexD recording system with A/D conversion at 40 kHz (16 bit). A digital head stage processing subsystem (Intan, 32 channel) passed continuous wide-band data referenced against the ground screws (low cutoff = 0.7 Hz) to a hard drive using PlexControl data acquisition software. For analysis of LFP recordings, wideband data was down-sampled to 2 kHz. A maximum of one channel per tetrode was included in our analyses, and twelve tetrodes were excluded for poor signal. As a result of these restrictions, 30 channels recorded from Pb^{2+}-exposed rats were analyzed, and 30 channels from control animals were analyzed. All of the selected channels were included in all analyses, providing a robust sampling of hippocampal recording sites for each group.

Behavioral tracking. The physical and software settings for the two video cameras used for behavioral tracking were tuned independently to optimize detection of body contours on one camera and to optimize tracking of head-mounted LEDs on the other. LED tracking entailed tabulating the coordinates of two clusters of LED florets (one green and one blue) that were offset ~2 cm laterally from the head-stage at ~3 cm above the rat's head. Each LED cluster comprised three florets oriented upward and slightly outward. This construction enabled consistent LED tracking despite behaviors in which rats oriented their heads away from the level plane. Body location was calculated from difference images obtained by subtracting an image of the empty arena from each frame capture during an experiment. Movement speeds were calculated from these body coordinates. The location of the head was calculated as the midpoint between the two LED clusters for each timepoint. Using Cineplex software (Plexon), LED tracking data was collected

online during experiments, and body contour tracking was derived offline from recorded videos. Video tracking frame captures (30 fps) were synchronized in real time to the simultaneously recorded neural data via a central timing board (Plexon).

Co-registration of LED and body tracking data. Following acquisition, all analyses of behavioral data were performed with custom-written Matlab scripts (MathWorks, Natick, MA). First, the coordinate system for camera one was mapped onto the coordinate system for camera two, enabling integration of the two types of tracking data. We then derived for each timestep the animal's head direction (HD) relative to the environment (from the axis between the two head-mounted LED clusters); body direction (BD) relative to the environment (from the midpoint between the LEDs to the center of the body); head angle (HA) relative to the body (using the LED axis relative to BD); and the rotational velocity of the body.

Definitions of running and stationary bouts. Rats exhibit a wide range of behaviors that involve body and head movements at substantial speeds. These movements appear in tracking data as changes in body and LED coordinates, just as running does. To isolate bouts of locomotion from other behaviors including grooming and rearing, we first required that movement speed be maintained above 5 cm/sec for a minimum duration of 1.025 or 2.05 seconds with a minimum peak speed of 15 cm/sec. We then eliminated all instances where head angle exceeded 35 degrees or body rotational velocity exceeded 52.5 degrees per second at any time. Stationary bouts were required to meet the same minimum duration, HA, and rotational criteria and not exceed a maximum movement speed of 5 cm/sec.

Derivation of oscillatory metrics. We evaluated the correspondence to animals' movement speeds of LFP dynamics in the delta-, theta-, and slow and fast gamma-frequency bands (1-4 Hz, 6-10 Hz, 25-55 Hz, and 65-120 Hz, respectively) using amplitude timeseries for each band and using the power spectral density of the LFP. We derived amplitude timeseries for each band by resampling to 2kHz the peak-to-trough amplitudes of each oscillatory cycle of the respective band-pass filtered LFPs. The spectral content of HC recordings was estimated using Welch's method for

each stationary and running bout. The 1.025 and 2.05 second minimum durations required in our bout definitions were chosen as a compromise between the relatively fast timescale of rats' locomotor behaviors, e.g. bouts of running and interspersed pauses, and the reduction in number of oscillatory cycles (particularly for delta) contributing to amplitude measures for shorter time windows.

Estimates of delta and theta power from the PSDs for individual behavioral bouts were defined as the mean values across the respective frequency ranges. For each recording site, delta and theta power estimates were defined as the medians of these values across all bouts of each type. Delta and theta peak frequencies and peak power estimates were measured directly from the PSDs for behavioral bouts. Scatterplots of these values are shown in Supplemental Figure 3. Correlation coefficients relating these measures to running speed were derived for each recording site across all bouts of each type. Distributions of these correlation coefficients for each group are shown in Supplemental Figure 4.

We defined behavioral modulation of oscillatory metrics as the difference between running bouts and stationary bouts. First, mean PSDs across bouts of each type were derived for each recording site. Then behavioral modulation was calculated for each site as the subtraction of the mean stationary PSD from the mean running PSD. Behavioral modulation for each site was then normalized either by the area of the mean stationary PSD or by dividing by the mean stationary PSD to give the percent change at each frequency (as in Figure 2D). Behavioral modulation of delta and theta were defined as the mean values across the respective bands for each recording site.

To further evaluate the effects of Pb^{2+} exposure on oscillatory synchronization in each frequency band, we collected peak-to-trough amplitude measurements for every cycle of band-pass filtered LFPs for each recording site for all bouts of each type. The normalized distributions of these amplitude measurements are plotted in Supplemental Figure 6.

Seizure Detection. We observed spike-wave discharges (SWDs) in Pb^{2+}-exposed rats as well as at least one control rat (Figs.1&3, Supp. Fig. 2). Representative examples of these events

consisted of large-amplitude oscillations, plainly recognizable in the LFP, with a fundamental frequency in the theta-band and several theta harmonics that were prominent in the spectrogram (Fig. 3). SWDs occurred when animals were stationary, supporting the view that SWDs are the physiological manifestations of 'absence' seizures. To compare the incidence of SWDs between Pb^{2+}-exposed rats and controls, we developed a detection algorithm based on the frequency composition of the short time-windowed LFP. Using windows of two seconds (one second overlap) we first derived power estimates within a 2 Hz frequency range centered on the frequency of peak theta power (5-14 Hz), and within 2 Hz ranges centered on the first and second harmonics of the theta-peak frequency. For each of these frequency bands, we took the z-scored values across all time windows throughout each session. Negative values in these timeseries were zeroed yielding metrics of elevated theta and theta harmonic power. These metrics and the time-averaged LFP amplitude were smoothed with a Gaussian and their product was z-scored to give a timeseries that was effective at identifying most SWDs of reasonable strength. This detection timeseries was also effective at identifying moments of particularly strong theta and theta-harmonic power during running. We categorized detection peaks as SWDs when they exceeded threshold values of 0.5-4 and only when average movement speeds were below 5 cm/sec within the corresponding PSD windows. The incidence, strength, and durations of SWDs were then compared between Pb^{2+}-exposed animals and controls.

PPI experiments. Pre-pulse inhibition of acoustic startle (PPI) was assessed in male and female rats at PN28, PN50, and PN120 following a protocol adapted from Abazyan et al. (2014). Four identical SR-LAB startle chambers (San Diego Instruments Inc., San Diego, CA, USA) were used to measure startle responses. Rats were placed inside the startle chamber into a mounted Plexiglas® cylinder with an accelerometer. Broadband background noise and acoustic stimuli were delivered via a speaker on the ceiling of the chamber. Sound levels were calibrated using a digital sound level meter, and accelerometer sensitivities for each chamber were calibrated daily. Presentation of acoustic stimuli was controlled by the SR-LAB software and interface system, and

accelerometer measurements were recorded. Each experimental session started with a five-minute period during which rats acclimatized to 68 dB background noise that was continuous throughout the session. Next, rats' average startle responses were calculated as the mean of 10 acoustic pulses (120dB, 100ms) presented at a random inter-trial intervals. Rats were left in the enclosure for an additional five minutes prior to beginning PPI trials. Rats were exposed to the following trial types: pulse-alone trial (120dB, 100ms); pre-pulse alone (90dB, 20ms); and four pre-pulse–pulse combinations (20 ms pre-pulse presented 80 ms before the 120 dB, 100 ms pulse) using one of the five pre-pulse intensities: 74, 78, 82, 86 and 90 dB. Each session consisted of six presentations of each trial type presented in a pseudorandom order with random inter-trial intervals. The average response during the 100 ms recording window beginning at stimulus onset was used as the measure of startle responses. PPI was quantified for each animal as the percent change in startle amplitude on pre-pulse–pulse trials relative to pulse-alone trials.

Blood Pb^{2+} Levels. Blood Pb^{2+} levels of rats used in PPI experiments (Table 1) were measured in samples obtained from cardiac puncture under sodium pentobarbital anesthesia. Samples were prepared and measured following protocols provided using the LeadCare Plus system (Magellan Diagnostics, N. Billerica, MA).

Histology. At the completion of data collection, rats used in electrophysiological experiments were anesthetized with isoflurane (5%) mixed with oxygen (800 ml/min) and marking lesions were made with a NanoZ (Plexon) to deliver 10μA for 10s at each electrode locations. About an hour later, rats were transcardially perfused with 100 ml phosphate-buffered saline (PBS), followed by 200 ml of 4% paraformaldehyde (PFA, pH 7.4; Sigma-Aldrich, St. Louis, MO). Blood Pb^{2+} levels of these rats were measured in samples obtained from cardiac puncture during the perfusion. Brains were post-fixed overnight in 4% PFA and then placed in a 30% sucrose solution for cryoprotection. Frozen brains were cut on a Leica CM3050 S cryostat (40 μm; coronal) and Nissl-stained. Marking lesions were mapped onto plates of the Paxinos & Watson Atlas (2004).

Results

We assessed the impact of Pb^{2+} neurotoxicity on hippocampal network synchronization by comparing the spectral content of local field potential (LFP) recordings from rats chronically exposed to Pb^{2+} and control animals as they freely explored a large 'open field' environment (Fig.1).

Normal behavior and power spectra in Pb^{2+}-exposed animals. We found no effect of Pb^{2+} exposure on continuous measures of locomotor behavior including movement speed, spatial orientation (body and head direction), and rotational velocity, nor did we find differences in behavioral measures that sampled distinct bouts of running and immobility as defined in Schultheiss et al. (2020) (Supp. Fig. 1). Spectrograms illustrating the time-frequency decomposition of hippocampal LFPs were also qualitatively similar between Pb^{2+}-exposed rats and control animals (e.g. Fig. 1E vs F top left), showing elevated theta power (5-14 Hz) coincident with running (green arrows) and elevated delta power (1-4 Hz) during immobility (cyan arrows). This observation suggests that chronic, low-level Pb^{2+} exposure does not disrupt hippocampal dynamics so severely as to eliminate the fundamental orthogonal modes that encode alternating segments of locomotion and stationary behavior during episodes of spatial navigation (Schultheiss et al., 2020).

In addition to quasi-normal delta- and theta-dominated hippocampal network modes, in both Pb^{2+}-exposed and normal animals we observed sporadic instances of maximal theta-frequency network synchronization accompanied by striking theta harmonics (Fig. 1F, right panel; timing indicated in left panel, red arrowhead). Raw LFP traces giving rise to these theta-harmonic events were excellent matches to *spike-wave discharges* that are the neurophysiological manifestations of 'absence seizures' in many epilepsies. We observed absence seizures in all eight Pb^{2+}-exposed rats during periods of immobility (Fig. 1F), and in line with previous observations (Taylor et al., 2019, Rodgers et al., 2015, Letts et al., 2014, Pearce et al., 2014) spike-wave discharges were also evident in a minority of control rats (Supp. Fig. 2).

As anticipated from session spectrograms (Fig. 1), power spectra of hippocampal LFPs showed qualitatively similar relationships of delta- and theta-band power to locomotor behavior in

both Pb^{2+}-exposed animals and controls (Fig. 2A&B). Cycle-by-cycle amplitudes of delta-, theta-, and fast gamma-frequency oscillations were also consistently modulated by movement speed in both groups (Figure 2C).

Theta hypersynchrony. Importantly, theta-synchronization was markedly elevated during both stationary bouts (1 sec bouts: p=0.01, t=-2.6, df=58; 2 sec bouts: p=0.04, t=-2.1, df=58) and running bouts (1 sec: p=0.002, t=-2.8, df=58; 2 sec: p=0.002, t=-3.2, df=58) (Fig. 2B). Moreover, stronger speed modulation of theta further increased theta synchrony (Fig. 2D).

We also found that theta frequency was substantially lower in Pb^{2+}-exposed rats compared to controls during both stationary bouts (control: 7.2 ± 1.1, Pb: 6.8 ± 1.0; $p=8.1x10^{-6}$, t=-4.5, df=842) and running bouts (control: 8.2 ± 0.4, Pb: 7.8 ± 0.6; $p=3.9x10^{-25}$, t=-10.77, df=702) (Supp. Fig. 3).

Pairwise 2-D scatterplots of theta power, theta frequency, and running speed for each bout type suggest that (1) covariation of theta power and theta frequency was disrupted in Pb^{2+}-exposed rats relative to controls (Supp. Fig. 3A), right; green vs black lines); and (2) running speed modulation of theta frequency was confined to a narrower range of speeds (Supp. Fig. 3B, right; green vs black lines); and in contrast, (3) running speed modulation of theta power occupied similar parameter spaces in Pb^{2+}-exposed rats and controls (Supp. Fig. 3C, right; green vs black lines).

Comparison of distributions of correlation coefficients confirmed the expected positive correlations of theta power and frequency to running speed for the majority of recording sites in both Pb^{2+}-exposed rats and controls (Supp. Fig. 4). Importantly, we also found that the correlation of theta power to running speed was heightened in Pb^{2+}-exposed rats relative to controls (p=0.0149, t=2.511, df=58), potentially reflecting a reduction in the dimensionality of hippocampal representations in favor of locomotor parameters, i.e. limiting the integration of multidimensional information arriving at the hippocampus from widespread cortical regions. However, in contrast to the apparent restriction of running speed modulation of theta frequency to a narrower range of speeds in Pb^{2+}-exposed rats, we found that correlations between running speed and theta frequency were similar in strength between groups (Supp. Fig. 4C, top vs bottom; p=0.192, t=-

1.319, df=58). Taken together, these observations suggest that Pb^{2+} exposure leading to theta hypersynchrony may impact the fidelity of relationships between theta dynamics and locomotion.

Delta power in Pb^{2+}-exposed rats was also elevated relative to controls during two second stationary bouts (p=0.05, t=-2.1, df=58), but this trend was weak for one second bouts that are generally more strongly impacted by behavioral variability (p=0.14, t=-1.5, df=58) (Fig. 2B). No differences in delta power between groups were observed during running. Interestingly, linear fits to delta power across individual recording sites from each rat revealed a consistent distal-proximal gradient of increasing delta power in control animals that was not evident in Pb^{2+}-exposed animals (Supp. Fig. 5).

Next, we evaluated differences in behavioral modulation of the PSD between Pb^{2+}-exposed rats and controls by comparing mean PSDs for stationary bouts (normalized by the integral of the PSD) to the corresponding mean PSDs for running bouts for each recording site. This approach yielded 'difference spectra' that revealed stronger behavioral modulation of theta and the first harmonic of theta in Pb^{2+}-exposed animals relative to controls (Fig. 2D). Augmentation of the difference in theta synchronization between behavioral states may reflect increased susceptibility of HC to entrainment by theta rhythmic inputs recruited during running or to self-organization of theta oscillations with hippocampal excitation. This analysis also revealed a possible reduction of behavioral modulation of relative oscillatory power in the 40-60 Hz range.

Effect of Pb^{2+} exposure on oscillatory cycle amplitudes. Analysis of PSDs are not well suited to address potential effects of Pb^{2+} on gamma-band oscillations. Therefore, to evaluate the impact of Pb^{2+} on gamma synchronization, and to further explore delta and theta effects, for each frequency band we compiled the distributions of the peak-to-trough amplitudes of individual cycles during stationary and running bouts. As expected, delta, theta, and fast gamma amplitudes were all strongly modulated by behavior for control rats and for Pb^{2+}-exposed rats, and slow gamma did not show differences in amplitude between bout types (Supp. Fig. 6, mirroring Fig. 2C). Comparisons of Pb^{2+}-exposed rats to controls demonstrated pronounced increases in cycle amplitudes for theta-

and gamma-frequency bands during stationary bouts (theta: $p=1.4x10^{-236}$, t=-32.9, df=114,635; slow gamma: p=0, t=-78.2, df=554,144; fast gamma: p=0, t=-168.2, df=1,276,491) and during running bouts (theta: p=0, t=-116.5, df=102,653; slow gamma: p=0, t=-90.5, df=491,214; fast gamma: p=0, t=-101.32, df=1,127,377). Although statistically significant, differences in delta cycle amplitudes between Pb^{2+}-exposed rats and controls were small relative to those for theta and gamma (stationary: $p=2.9x10^{-8}$, t=-5.5, df=41741; running: $p=1.9x10^{-16}$, t=8.2, df=34211); and it is important to consider that with such large numbers of individual cycle amplitude measurements for each frequency band, statistical significance may not be informative.

Pb^{2+} exposure exacerbates absence seizures. As noted earlier, both Pb^{2+}-exposed animals and controls exhibited absence seizures during immobility (Fig. 1), and these events were characterized by spike-wave discharges in the LFP (Fig. 3A) and maximal theta-frequency synchronization with several harmonics appearing in spectrograms (Fig. 3B). These seizure events often created a considerable right tail in distributions of theta power estimates during immobility (Fig. 3C). In many cases theta power distributions were bimodal (Fig. 3C, inset) such that the lowest theta values corresponded to quiet-wakeful immobility; intermediate and larger values corresponded to elevated theta during running; and theta values during SWDs were on the order of the maximal theta during fast running (Fig. 3D, left). Recordings at sites exhibiting weaker theta enabled easy detection of SWDs (Fig. 3D, right) with a single threshold for theta power or also using thresholded estimates of power at the first harmonic of theta (Fig. 3D, right, insets). We recently characterized delta-dominated hippocampal network activity during intermittent locomotion as a fundamental mode of encoding or segmenting events within a behavioral episode. Seizures were uniformly distinct from delta states during immobility, exhibiting minimal delta power (Fig. 3E). Interestingly, strong delta synchronization was often observed to flank seizures in the spectrogram occurring at the onset or offset (Fig. 3B, red arrowheads), as has been suggested could aid seizure prediction in a clinical setting.

Given the variability in the spectral content of recordings at different hippocampal sites (as in Fig. 3D, left vs right), discerning the spectral signature of SWDs could be a greater or lesser challenge. Using a novel seizure-detection algorithm that integrates the self-normalized (z-scored over time) power at theta frequency and at the first two harmonics of theta with the concurrent LFP signal amplitude, we were able to detect with high reliability spike-wave discharges occurring during immobility (Fig. 3F). We would argue these are likely to have been absence seizures (Fig. 3B&F). By varying the detection threshold applied to this algorithm we found a broad range of values for which the detected events could be visually confirmed. The range across which the algorithm performed well was bounded below by false positives where the algorithm identified other instances of theta harmonic activity, typically during running, in addition to spike-wave discharges. We reduced the majority of false positives by implementing a requirement that the animal be stationary at the time of the theta-harmonic event. The algorithm's functional range was bounded above by false negative where the algorithm identified only spike-wave discharges but missed some proportion of the true incidence. Across the 8-fold range of good performance (0.5 to greater than 4), Pb^{2+}-exposed rats exhibited *normal* SWDs (with the same theta fundamental frequency) that were of significantly greater strength; that were of longer duration; and that occurred during a greater proportion of rats' time spent stationary (Fig. 3G). Typical doses of ethosuximide (100-200 mg/kg), a preferred drug for absence epilepsy, completely abolished seizures (Fig. 3H).

Disruption of sensorimotor gating. In a last series of experiments, we tested the effect of Pb^{2+} exposure on PPI of acoustic startle, an assay of sensorimotor gating known to be impaired in adults with schizophrenia. Figure 4 shows the pattern of results analyzed in males and females across development (PN28, PN50, and PN120). We tested the baseline acoustic startle responses in all groups and found no significant differences (all t-test p's >0.05), suggesting any differences observed in PPI reflect sensory-motor gating.

Males. We found effects of Pb2+-exposure in adult males (PN50 and PN120), but not at PN28, demonstrating a developmental trajectory for the emergence of PPI deficits that is similar to

schizophrenia. At PN28, a two-way ANOVA showed a main effect of dB level ($F_{2.57, 89.83}$=68.89, p<0.001), no main effect of Pb2+-exposure ($F_{1,35}$ =0.54, p=0.467), and no level x exposure interaction ($F_{2.57, 89.83}$=2.56, p=0.069). At PN50, there was a main effect dB level ($F_{3.12, 109.23}$=53.49, p<0.001), a main effect of Pb2+-exposure ($F_{1,35}$=11.32, p<0.01), but no level x exposure interaction ($F_{3.12, 109.23}$=1.34, p=0.266). At PN120, there was a main effect dB level ($F_{2.88, 115.11}$=59.59, p<0.001), a main effect of Pb2+-exposure ($F_{1,35}$=9.30, p<0.01), but no level x exposure interaction ($F_{2.88, 115.11}$=2.00, p=0.120).

Females. We found no effects of Pb2+-exposure in female rats at any age. At PN28, a two-way ANOVA showed a main effect of dB level ($F_{2.56, 92.28}$=42.74, p<0.001), no main effect of Pb2+-exposure ($F_{1,36}$ =0.01, p=0.942), and no level x exposure interaction ($F_{2.56, 92.28}$=0.17, p=0.888). At PN50, there was a main effect dB level ($F_{2.89, 101.26}$=90.26, p<0.001), no main effect of Pb2+-exposure ($F_{1,35}$=0.28, p=0.602), and no level x exposure interaction ($F_{2.89, 101.26}$=0.61, p=0.606). At PN120, there was a main effect dB level ($F_{2.82, 104.17}$=57.96, p<0.001), no main effect of Pb2+-exposure ($F_{1,37}$=0.02, p=0.878), and no level x exposure interaction ($F_{2.82, 104.17}$=0.61, p=0.597).

Discussion

We analyzed the spectral content of hippocampal LFPs and found that rats chronically exposed to Pb^{2+} exhibited multiple forms of theta-frequency hypersynchrony including absence seizures with a fundamental frequency in the theta-band and multiple theta harmonics extending well into the gamma frequency range. Heightened behavioral modulation of theta synchrony was also observed, but modulation was restricted to a narrower range of locomotor parameters suggesting that excess theta synchrony caused by Pb^{2+} exposure diminishes the encoding capacity of hippocampal networks. We also found that theta frequency was lower in Pb^{2+}-exposed rats during both running and immobility. Slower frequency oscillations are generally associated with synchronization of larger populations of neurons, and intrinsic coupling within hippocampal networks and active membrane properties of hippocampal neurons are well suited to self-organize theta-rhythmic activity (Goutagny et al., 2009, Stark et al., 2015). Lower frequency theta could

492 therefore reflect the broader synchronization of hippocampal networks, entraining a higher
493 proportion of neurons, and restricting hippocampal functional capacity by reducing the number and
494 flexibility of network states available. Importantly, parvalbumin expressing interneurons (PVGIs) are
495 major contributors to theta rhythmic synchronization of hippocampal principal cells (Amilhon et al.,
496 2015), but PVGIs are reduced in animals chronically exposed to Pb^{2+}. One potential explanation of
497 this inconsistency is that the reduction in number is compensated for by increased local connectivity
498 of the remaining PVGIs to maintain an appropriate excitatory-inhibitory balance within hippocampal
499 networks. Such a homeostatic function might endow the remaining PVGIs with stronger influence
500 over the spike timing of larger populations of synaptic targets leading to excessive synchrony.
501 Interestingly, ablation of NMDARs on PVGIs (presumably without reducing PVGI number) yields the
502 opposite pattern of effects on theta than Pb^{2+} exposure, increasing theta frequency while reducing
503 power, and resulting in disrupted hippocampal representations and impaired memory (Korotkova et
504 al., 2010).

505 As we have recently demonstrated, distinct modes of delta- and theta-dominated
506 hippocampal network activity can transition rapidly in tandem with the stops and starts of rats'
507 locomotor trajectories. In that study delta and theta power were orthogonal across modes such that
508 strong delta synchronization occurred when theta was weak and vice versus. This pattern of
509 exclusivity between hippocampal modes may reflect distinct neurophysiological processes or
510 cognitive functions contributing to spatial navigation and memory (Schultheiss et al., 2020). Thus, to
511 minimize blurring the oscillatory dynamics of distinct modes that accompany behaviors occurring in
512 rapid succession, we focused our subsequent analyses on hippocampal synchronization during the
513 precisely-defined stationary and running bouts.

514 *Absence seizures.* Absence seizures manifested as spike-wave discharges in the
515 hippocampal LFP were exhibited by all Pb^{2+}-exposed animals and a minority of control animals.
516 Comparisons between groups showed that Pb^{2+}-exposure greatly increased the likelihood and
517 incidence of seizures, exacerbated the intensity of seizures, increased seizure durations, and

increased the proportion of time spent stationary during which seizures occurred. It is provocative to consider that the theta-band fundamental frequency of SWDs may reflect pathological engagement of theta rhythmogenic mechanisms that are normally the foundation of spatial encoding and episodic memory systems. Given the complementary observations of theta hypersynchrony during locomotor behavior and heightened behavioral modulation of theta, we would argue that disrupted theta rhythmic coordination of hippocampal networks is a key consequence of Pb^{2+} neurotoxicity. Since elevated theta has also been found to correspond to disruption of sensory motor gating in schizophrenia, and Pb2+ exposure is a risk factor for both schizophrenia and epilepsy; perhaps theta rhythmogenic mechanisms are the common element to all three conditions.

In addition to theta hypersynchrony, we also found increased gamma-frequency synchronization in Pb^{2+}-exposed animals. Elevated gamma activity in normal animals is integral to cognitive processes including attention, perception, and memory encoding (e.g. Fell et al., 2001, Jutras et al., 2009, Yamamoto et al., 2014, Fries et al., 2001), but Pb^{2+}-exposed animals show deficits in cognition and memory. One possibility is that the elevated gamma synchronization seen in Pb^{2+}-exposed animals is in fact a consequence of the excessive theta synchrony that we have described. Pastoll and colleagues (2013) showed that theta-frequency excitation of layer II of medial entorhinal cortex *in vitro* was sufficient to elicit well-timed gamma oscillations nested with theta cycles. This demonstrates that the local microcircuitry responsible for gamma synchronization can be engaged by theta-rhythmic excitation in the absence of an intact animal, and this mechanism could be strongly driven by theta hypersynchrony in Pb^{2+}-exposed animals.

Importantly, hypersynchrony reflects reduced stochasticity in network dynamics which can be detrimental to encoding capacity and flexibility. We further observed increased behavioral modulation of theta power. It is important to note that this is not behavioral modulation of encoding but rather a greater increase in theta synchronization that could reflect a further decrease in encoding capacity or flexibility during running. For example, single neurons in parahippocampal structures commonly show conjunctive representations of multiple spatial dimensions. When the

spatial tuning of conjunctive grid-head direction cells in medial entorhinal cortex is disrupted by inactivation of the medial septum, the fidelity of those cells for head direction tuning is increased (Brandon et al., 2013). Here, we revealed greater fidelity of theta power to running speed, which may also reflect a reduction in the dimensionality of hippocampal encoding. This pattern of effects would be consistent with reduced integration of information types or modalities of sensory input accompanying elevated entrainment of hippocampal populations to theta and stronger encoding fidelity for running speed. This interpretation could also incorporate our finding of disrupted sensorimotor gating resulting from Pb^{2+} exposure. If the hippocampus is excessively involved in encoding behavior, it may be less receptive to incoming sensory information. Furthermore, Pb^{2+} neurotoxicity and schizophrenia are both related to behavioral inflexibility or cognitive-behavioral perseveration consistent with this general formulation.

Related to the hypersynchrony observed here, Pb^{2+} exposure has been shown to increase the likelihood of epilepsy six-fold (Chang et al., 2011; Clark et al., 2012). Epilepsy is defined by its manifestation of neural hypersynchrony that can be either focal or global. Taking epilepsy as a model, hypersynchrony can cause specific or general cognitive deficits corresponding to focal or global appearances, in addition to the damaging effects of the seizure events on network architecture and dynamics resulting from dysfunctional plasticity resulting from hypersynchrony.

Though a lesser effect, we also note that there were interesting correlations of delta parameters to running speed in Pb2+-exposed rats when delta would normally be expected to be weak (as we previously described, Schultheiss et al., 2020). However, in addition to typical orthogonality between delta- and theta-dominated modes, we sometimes observed apparent correlations between frequency-bands occurring within a given network mode (such as high delta *and* high theta). See Figure 5 insets in Schultheiss et al., (2020). This suggests that Pb^{2+}-exposure may also cause atypical cross-frequency couplings that are detrimental to cognition and behavior.

Our findings strongly implicate multiple forms of theta-rhythmic hypersynchrony in hippocampus (HC), as well as amplified behavioral modulation of hippocampal theta, as

fundamental neurophysiological consequences of Pb^{2+} neurotoxicity. We suggest that hippocampal networks and/or septohippocampal circuit mechanisms of theta-generation become hyperactive as a consequence of Pb^{2+} exposure, likely reflecting altered synaptic coupling strengths and topology that imbalance dynamics towards theta-dominated activity. The conceptual framework that we propose base on these insights predicts that cognitive impairments resulting from chronic Pb^{2+} exposure and aspects of comorbid schizophrenia and epilepsy share etiological underpinnings whereby strengthened mechanisms of theta rhythmogenesis overpower normal intra-hippocampal network dynamics disrupting the functional efficacy of cortico-hippocampal circuits.

References

Abazyan, B., Dziedzic, J., Hua, K., Abazyan, S., Yang, C., Mori, S., Pletnikov, M. V., & Guilarte, T. R. (2014). Chronic exposure of mutant DISC1 mice to lead produces sex-dependent abnormalities consistent with schizophrenia and related mental disorders: a gene-environment interaction study. *Schizophrenia bulletin*, *40*(3), 575–584. https://doi.org/10.1093/schbul/sbt071

Amilhon, B., Huh, C. Y., Manseau, F., Ducharme, G., Nichol, H., Adamantidis, A., & Williams, S. (2015). Parvalbumin Interneurons of Hippocampus Tune Population Activity at Theta Frequency. Neuron, 86(5), 1277–1289. https://doi.org/10.1016/j.neuron.2015.05.027

Arbab, T., Battaglia, F. P., Pennartz, C., & Bosman, C. A. (2018). Abnormal hippocampal theta and gamma hypersynchrony produces network and spike timing disturbances in the Fmr1-KO mouse model of Fragile X syndrome. *Neurobiology of disease*, *114*, 65–73. https://doi.org/10.1016/j.nbd.2018.02.011

Bast, T., Zhang, W. N., & Feldon, J. (2001a). Hyperactivity, decreased startle reactivity, and disrupted prepulse inhibition following disinhibition of the rat ventral hippocampus by the GABA(A) receptor antagonist picrotoxin. *Psychopharmacology*, *156*(2-3), 225–233. https://doi.org/10.1007/s002130100775

Bast, T., Zhang, W. N., Heidbreder, C., & Feldon, J. (2001b). Hyperactivity and disruption of prepulse inhibition induced by N-methyl-D-aspartate stimulation of the ventral hippocampus and the effects of pretreatment with haloperidol and clozapine. *Neuroscience*, *103*(2), 325–335. https://doi.org/10.1016/s0306-4522(00)00589-3

Bast, T., & Feldon, J. (2003). Hippocampal modulation of sensorimotor processes. *Progress in neurobiology*, *70*(4), 319–345. https://doi.org/10.1016/s0301-0082(03)00112-6

Brandon, M. P., Bogaard, A. R., Schultheiss, N. W., & Hasselmo, M. E. (2013). Segregation of cortical head direction cell assemblies on alternating θ cycles. Nature neuroscience, 16(6), 739–748. https://doi.org/10.1038/nn.3383

Brubaker, C. J., Dietrich, K. N., Lanphear, B. P., & Cecil, K. M. (2010). The influence of age of lead exposure on adult gray matter volume. *Neurotoxicology*, *31*(3), 259–266. https://doi.org/10.1016/j.neuro.2010.03.004

Caito, S., & Aschner, M. (2017). Developmental Neurotoxicity of Lead. *Advances in neurobiology*, *18*, 3–12. https://doi.org/10.1007/978-3-319-60189-2_1

Canfield, R. L., Henderson, C. R., Jr, Cory-Slechta, D. A., Cox, C., Jusko, T. A., & Lanphear, B. P. (2003). Intellectual impairment in children with blood lead concentrations below 10 microg per deciliter. *The New England journal of medicine*, *348*(16), 1517–1526. https://doi.org/10.1056/NEJMoa022848

Cao, X., Huang, S., & Ruan, D. (2008). Enriched environment restores impaired hippocampal long-term potentiation and water maze performance induced by developmental lead exposure in rats. *Developmental psychobiology*, *50*(3), 307–313. https://doi.org/10.1002/dev.20287

Chang, Y. T., Chen, P. C., Tsai, I. J., Sung, F. C., Chin, Z. N., Kuo, H. T., Tsai, C. H., & Chou, I. C. (2011). Bidirectional relation between schizophrenia and epilepsy: a population-based retrospective cohort study. *Epilepsia*, *52*(11), 2036–2042. https://doi.org/10.1111/j.1528-1167.2011.03268.x

Clarke, M. C., Tanskanen, A., Huttunen, M. O., Clancy, M., Cotter, D. R., & Cannon, M. (2012). Evidence for shared susceptibility to epilepsy and psychosis: a population-based family study. *Biological psychiatry*, *71*(9), 836–839. https://doi.org/10.1016/j.biopsych.2012.01.011

Fries, P., Reynolds, J. H., Rorie, A. E., & Desimone, R. (2001). Modulation of oscillatory neuronal synchronization by selective visual attention. *Science* (New York, N.Y.), 291(5508), 1560–1563. https://doi.org/10.1126/science.1055465

Goutagny, R., Jackson, J., & Williams, S. (2009). Self-generated theta oscillations in the hippocampus. *Nature neuroscience*, *12*(12), 1491–1493. https://doi.org/10.1038/nn.2440

628 Guilarte, T. R., Opler, M., & Pletnikov, M. (2012). Is lead exposure in early life an
629 environmental risk factor for Schizophrenia? Neurobiological connections and testable
630 hypotheses. *Neurotoxicology*, *33*(3), 560–574. https://doi.org/10.1016/j.neuro.2011.11.008
631 Guilarte T. R. (1997). Pb2+ inhibits NMDA receptor function at high and low affinity sites:
632 developmental and regional brain expression. *Neurotoxicology*, *18*(1), 43–51.
633 Guilarte, T. R., Miceli, R. C., Altmann, L., Weinsberg, F., Winneke, G., & Wiegand, H.
634 (1993). Chronic prenatal and postnatal Pb2+ exposure increases [3H]MK801 binding sites in adult
635 rat forebrain. *European journal of pharmacology*, *248*(3), 273–275. https://doi.org/10.1016/0926-
636 6917(93)90054-t
637 Guilarte, T. R., & Miceli, R. C. (1992). Age-dependent effects of lead on [3H]MK-801 binding
638 to the NMDA receptor-gated ionophore: in vitro and in vivo studies. *Neuroscience letters*, *148*(1-2),
639 27–30. https://doi.org/10.1016/0304-3940(92)90796-a
640 Guilarte, T. R., & McGlothan, J. L. (1998). Hippocampal NMDA receptor mRNA undergoes
641 subunit specific changes during developmental lead exposure. *Brain research*, *790*(1-2), 98–107.
642 https://doi.org/10.1016/s0006-8993(98)00054-7
643 Guilarte, T. R., Toscano, C. D., McGlothan, J. L., & Weaver, S. A. (2003). Environmental
644 enrichment reverses cognitive and molecular deficits induced by developmental lead
645 exposure. *Annals of neurology*, *53*(1), 50–56. https://doi.org/10.1002/ana.10399
646 Hashimoto, T., Volk, D. W., Eggan, S. M., Mirnics, K., Pierri, J. N., Sun, Z., Sampson, A. R.,
647 & Lewis, D. A. (2003). Gene expression deficits in a subclass of GABA neurons in the prefrontal
648 cortex of subjects with schizophrenia. *The Journal of neuroscience : the official journal of the*
649 *Society for Neuroscience*, *23*(15), 6315–6326. https://doi.org/10.1523/JNEUROSCI.23-15-
650 06315.2003
651 Jaako-Movits, K., Zharkovsky, T., Romantchik, O., Jurgenson, M., Merisalu, E., Heidmets, L.
652 T., & Zharkovsky, A. (2005). Developmental lead exposure impairs contextual fear conditioning and

653 reduces adult hippocampal neurogenesis in the rat brain. *Internat. J. of Dev. Neurosci.*, *23*(7), 627–
654 635. https://doi.org/10.1016/j.ijdevneu.2005.07.005
655 Jett, D. A., Kuhlmann, A. C., & Guilarte, T. R. (1997). Intrahippocampal administration of
656 lead (Pb) impairs performance of rats in the Morris water maze. *Pharmacology, biochemistry, and*
657 *behavior*, *57*(1-2), 263–269. https://doi.org/10.1016/s0091-3057(96)00349-8
658 Korotkova, T., Fuchs, E. C., Ponomarenko, A., von Engelhardt, J., & Monyer, H. (2010).
659 NMDA receptor ablation on parvalbumin-positive interneurons impairs hippocampal synchrony,
660 spatial representations, and working memory. *Neuron*, 68(3), 557–569.
661 https://doi.org/10.1016/j.neuron.2010.09.017
662 Kuhlmann, A. C., McGlothan, J. L., & Guilarte, T. R. (1997). Developmental lead exposure
663 causes spatial learning deficits in adult rats. *Neuroscience letters*, *233*(2-3), 101–104.
664 https://doi.org/10.1016/s0304-3940(97)00633-2
665 Letts, V.A., Beyer, B.J. and Frankel, W.N. (2014), Hidden in plain sight: spike-wave
666 discharges in mouse inbred strains. Genes, Brain and Behavior, 13: 519-526.
667 https://doi.org/10.1111/gbb.12142
668 McGlothan, J. L., Karcz-Kubicha, M., & Guilarte, T. R. (2008). Developmental lead exposure
669 impairs extinction of conditioned fear in young adult rats. *Neurotoxicology*, *29*(6), 1127–1130.
670 https://doi.org/10.1016/j.neuro.2008.06.010
671 Miranda, M. L., Kim, D., Galeano, M. A., Paul, C. J., Hull, A. P., & Morgan, S. P. (2007). The
672 relationship between early childhood blood lead levels and performance on end-of-grade
673 tests. *Environmental health perspectives*, *115*(8), 1242–1247. https://doi.org/10.1289/ehp.9994
674 Munoz, C., Garbe, K., Lilienthal, H., & Winneke, G. (1988). Significance of hippocampal
675 dysfunction in low level lead exposure of rats. *Neurotoxicology and teratology*, *10*(3), 245–253.
676 https://doi.org/10.1016/0892-0362(88)90024-4
677 Needleman H. L. (1983). Lead at low dose and the behavior of children. *Acta psychiatrica*
678 *Scandinavica. Supplementum*, *303*, 26–37. https://doi.org/10.1111/j.1600-0447.1983.tb00939.x

679 Needleman, H. L., McFarland, C., Ness, R. B., Fienberg, S. E., & Tobin, M. J. (2002). Bone
680 lead levels in adjudicated delinquents. A case control study. *Neurotoxicology and teratology*, *24*(6),
681 711–717. https://doi.org/10.1016/s0892-0362(02)00269-6
682 Needleman H. (2004). Lead poisoning. *Annual review of medicine*, *55*, 209–222.
683 https://doi.org/10.1146/annurev.med.55.091902.103653
684 Nihei, M. K., Desmond, N. L., McGlothan, J. L., Kuhlmann, A. C., & Guilarte, T. R. (2000). N-
685 methyl-D-aspartate receptor subunit changes are associated with lead-induced deficits of long-term
686 potentiation and spatial learning. *Neuroscience*, *99*(2), 233–242. https://doi.org/10.1016/s0306-
687 4522(00)00192-5
688 Opler, M. G., Brown, A. S., Graziano, J., Desai, M., Zheng, W., Schaefer, C., Factor-Litvak,
689 P., & Susser, E. S. (2004). Prenatal lead exposure, delta-aminolevulinic acid, and
690 schizophrenia. *Environmental health perspectives*, *112*(5), 548–552.
691 https://doi.org/10.1289/ehp.6777
692 Opler, M. G., Buka, S. L., Groeger, J., McKeague, I., Wei, C., Factor-Litvak, P., Bresnahan,
693 M., Graziano, J., Goldstein, J. M., Seidman, L. J., Brown, A. S., & Susser, E. S. (2008). Prenatal
694 exposure to lead, delta-aminolevulinic acid, and schizophrenia: further evidence. *Environmental*
695 *health perspectives*, *116*(11), 1586–1590. https://doi.org/10.1289/ehp.10464
696 Paxinos, G., and Watson, C. (2004). The rat brain in stereotaxic coordinates 5th Edition.
697 (Massachusetts: Academic Press).
698 Pearce, P. S., Friedman, D., LaFrancois, J. J., Iyengar, S. S., Fenton, A. A., MacLusky, N.
699 J., Scharfman, H. E. (2014). Spike–wave discharges in adult Sprague–Dawley rats and their
700 implications for animal models of temporal lobe epilepsy. Epilepsy & Behavior, 32, 121-131.
701 https://doi.org/10.1016/j.yebeh.2014.01.004
702 Rodgers, K. M., Dudek, F. E., & Barth, D. S.. (2015). Progressive, seizure-like, spike-wave
703 discharges are common in both injured and uninjured sprague-dawley rats: implications for the fluid

704 percussion injury model of post-traumatic epilepsy J. Neurosci. 35 (24) 9194-9204.
705 https://doi.org/10.1523/JNEUROSCI.0919-15.2015

706 Schultheiss, N.W., Schlecht, M., Jayachandran, M., Brooks, D.R., McGlothan, J.L., Guilarte,
707 T.R. & Allen, T.A. (2020). Awake delta and theta-rhythmic hippocampal network modes during
708 intermittent locomotion behaviors in the rat. *Behavioral Neuroscience.*

709 Stansfield, K. H., Ruby, K. N., Soares, B. D., McGlothan, J. L., Liu, X., & Guilarte, T. R.
710 (2015). Early-life lead exposure recapitulates the selective loss of parvalbumin-positive GABAergic
711 interneurons and subcortical dopamine system hyperactivity present in schizophrenia. *Translational*
712 *psychiatry*, *5*(3), e522. https://doi.org/10.1038/tp.2014.147

713 Stark, E., Eichler, R., Roux, L., Fujisawa, S., Rotstein, H. G., & Buzsáki, G. (2013).
714 Inhibition-induced theta resonance in cortical circuits. *Neuron*, *80*(5), 1263–1276.
715 https://doi.org/10.1016/j.neuron.2013.09.033

716 Taylor, J. A., Reuter. J. D., Kubiak, R. A., Mufford, T. T., Booth, C. J., Dudek, F. E., & Barth,
717 D. S. (2019). Spontaneous recurrent absence seizure-like events in wild-caught rats. J. Neurosci.,
718 39(24), 4829-4841. https://doi.org/10.1523/JNEUROSCI.1167-18.2019

719 Wang, T., Guan, R. L., Liu, M. C., Shen, X. F., Chen, J. Y., Zhao, M. G., & Luo, W. J. (2016).
720 Lead Exposure Impairs Hippocampus Related Learning and Memory by Altering Synaptic Plasticity
721 and Morphology During Juvenile Period. *Molecular neurobiology*, *53*(6), 3740–3752.
722 https://doi.org/10.1007/s12035-015-9312-1

723 Yamamoto J, Suh J, Takeuchi D, Tonegawa S. Successful execution of working memory
724 linked to synchronized high-frequency gamma oscillations. Cell. 2014;157(4):845-857.
725 https://doi:10.1016/j.cell.2014.04.009

726

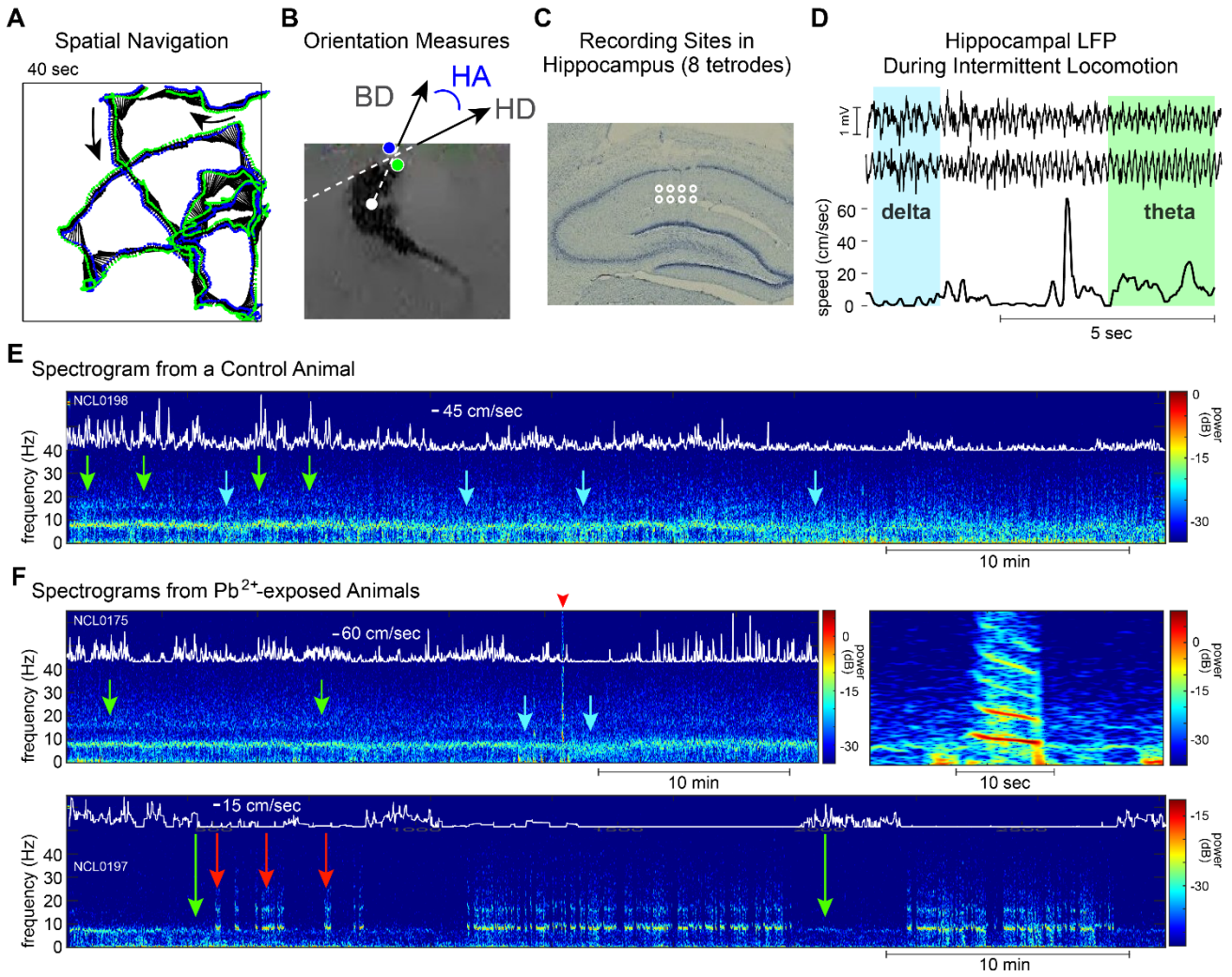

Figure 1. Hippocampal local field potentials (LFPs) during exploratory navigation show similar spectral content in Pb^{2+}-exposed rats as controls. A. Representative spatial trajectory during free exploration of the square (120 cm) 'open field' environment. Black lines represent the rat's body direction (BD as in **B**), and green and blue dots represent head-mounted LEDs. **B**. Continuous measures of locomotor behavior, including head direction relative to the environment (HD) and head angle (HA, derived from HD and BD). **C**. Recording sites of 8 tetrodes located at two depths on each of four shanks of a silicon probe. Tracks left by the shanks of the implanted probe are visible as disruptions of the CA1 cell layer. **D.** Representative LFP traces (top) during running and immobility (bottom) showed corresponding periods of strong theta and delta-band activity (e.g. as highlighted in cyan and green). **E&F**. Representative spectrograms for control rats (**E**) and Pb^{2+}-exposed rats (**F, top left panel**) showed qualitatively similar patterns of speed modulation (overlaid white traces) of theta (green arrows) and delta (cyan arrows). **F, top right panel**. Putative absence seizures occurred in all Pb^{2+}-exposed rats. Seizure incidence was highly variability across rats and across sessions for each rat, i.e. the spectrograms shown in **F** illustrate sessions during which a single seizure lasting 7 seconds and ~25 minutes of continuous seizing occurred (**top** and **bottom panels, respectively)**. The red arrowhead in the **top left** panel indicates the seizure magnified in the **top right** panel. Green arrows (**bottom panel**) indicate running accompanied by elevated theta power. Red arrows indicate seizure bouts during pauses in the rat's intermittent locomotor behaviors.

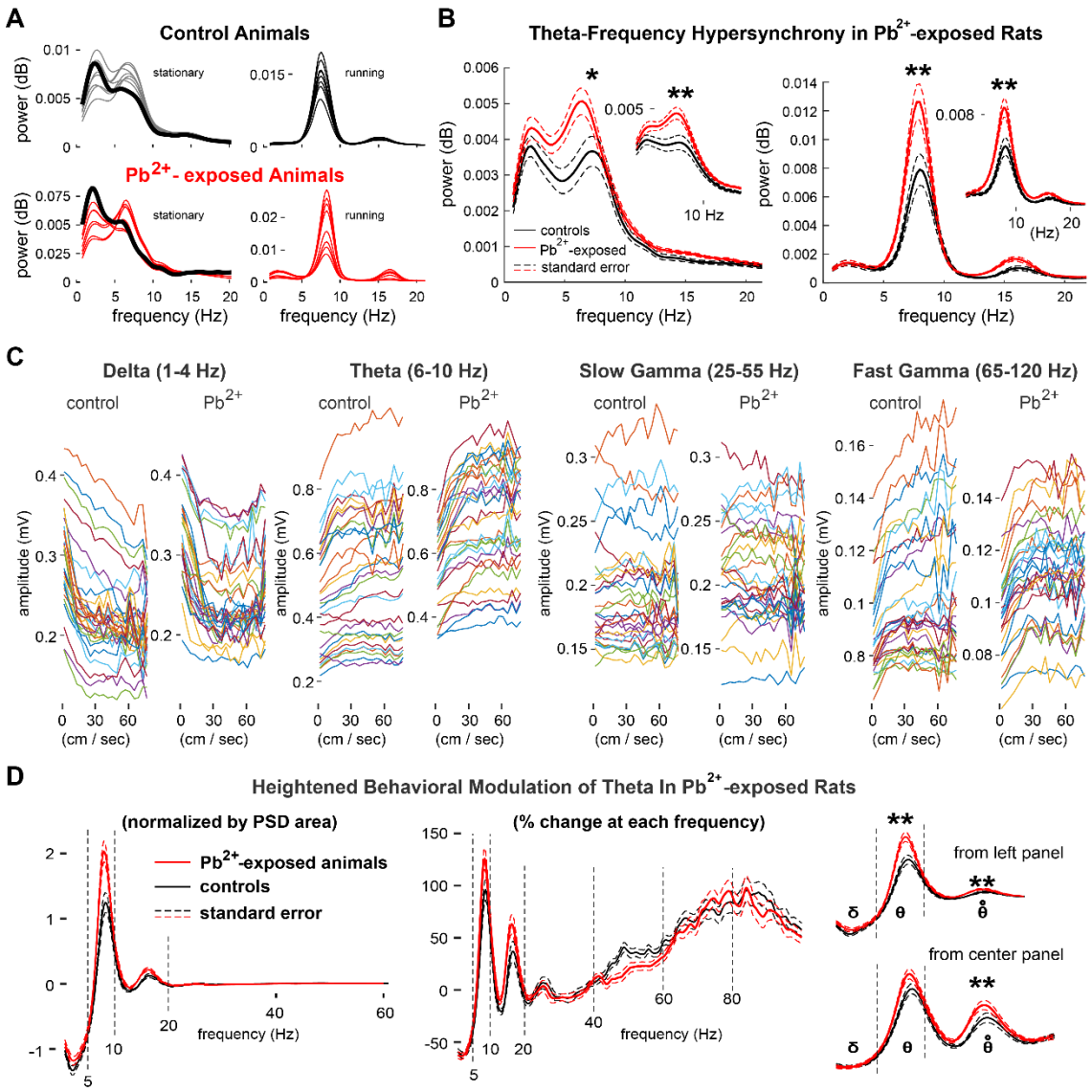

Figure 2. Theta-frequency hypersynchrony in Pb^{2+}-exposed rats. A. Power spectra (PSDs) of hippocampal LFPs both for Pb^{2+}-exposed rats and for controls exhibited diminished delta and heightened theta during running (**right**) relative to stationary bouts (**left**). Grey and red traces indicate representative PSDs of simultaneous recordings from each site in hippocampus. Thick black traces (**left panels**) are PSDs from the site with the highest delta power during immobility, highlighting the apparent tradeoff between delta and theta peaks across recording sites in each animal. **B**. Marked elevation of theta power in Pb^{2+}-exposed rats relative to controls (to >150%) during two second bouts of immobility (**left**) and running (**right**) (1 sec bouts **inset**). **C**. Similar patterns of movement speed modulation of cycle-by-cycle amplitudes of delta, theta, and gamma oscillations (across all behaviors) in Pb^{2+}-exposed rats and controls. **D**. Stronger behavioral modulation of theta power in Pb^{2+}-exposed rats than controls in terms of the absolute change (normalized by total power (0-25 Hz)) (**left**) and the relative change at each frequency (%) (**right**) between stationary and running bouts for control (black) and Pb^{2+}-exposed rats (red). Enlargement of the low frequency range of PSDs in left and center panels (**right**).

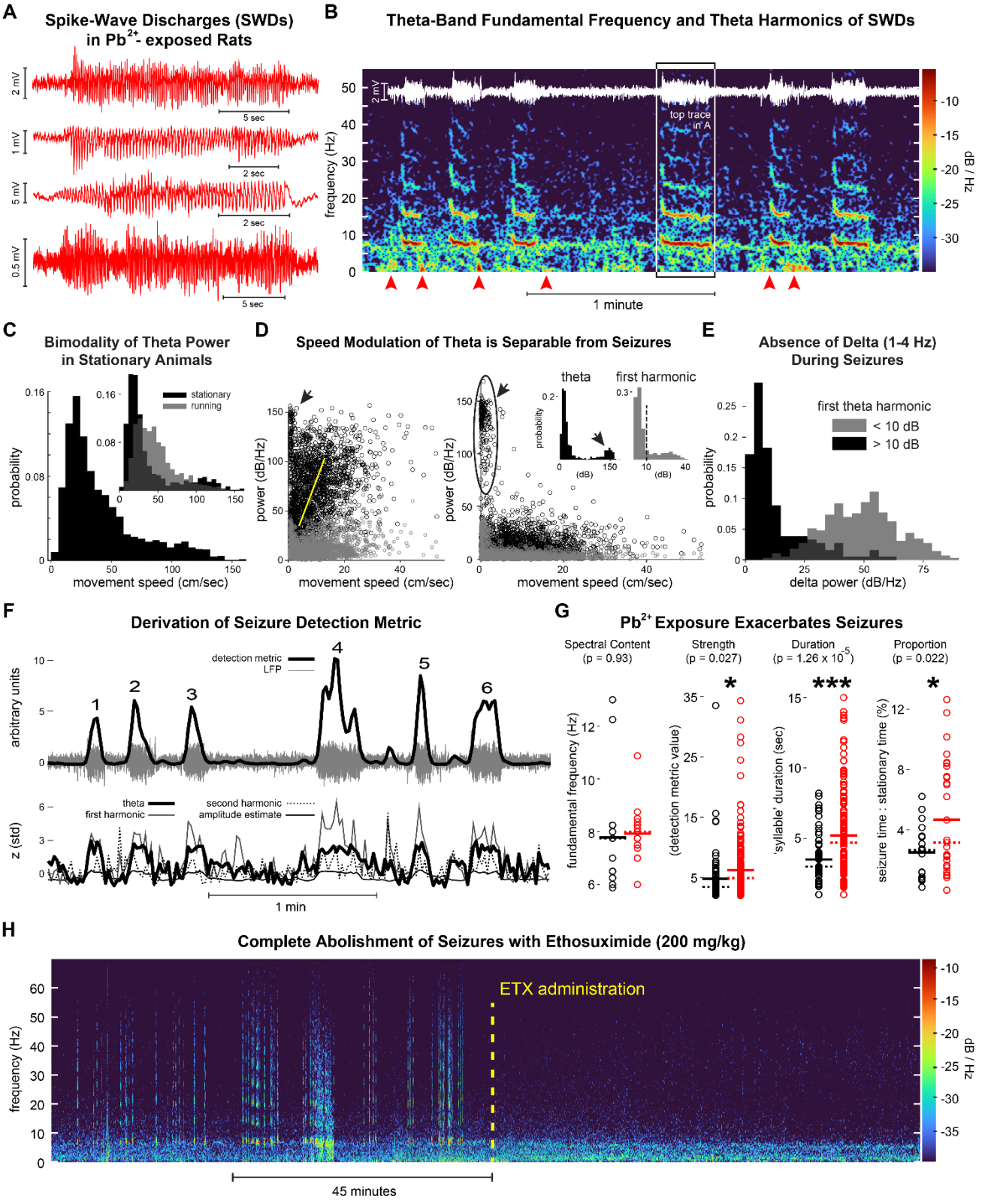

Figure 3. Chronic Pb^{2+} Exposure Exacerbates Hippocampal Absence Seizures. A. Spike-wave discharges (SWDs) in the hippocampal LFP from four Pb^{2+}-exposed rats. **B**. Spectrogram

showing six seizures. SWD overlaid in white. **C**. Theta power distributions during immobility showing evidence of numerous seizure events creating a pronounced right tail or second peak at high theta power values. **D**. The theta power to movement speed relationship shows cases where theta during seizures corresponds to maximal theta during fast running (left), and other cases where weaker theta draws into significant relief theta values corresponding to SWDs (right). Inset distributions of theta and harmonic power as in C. **E**. Delta synchronization was minimal when power at the first harmonic of theta was elevated. **F**. Derivation of the seizure detection algorithm. **G**. The theta fundamental frequency did not differ between groups, but Pb2+-exposed animals exhibited exacerbated seizure intensity and incidence.

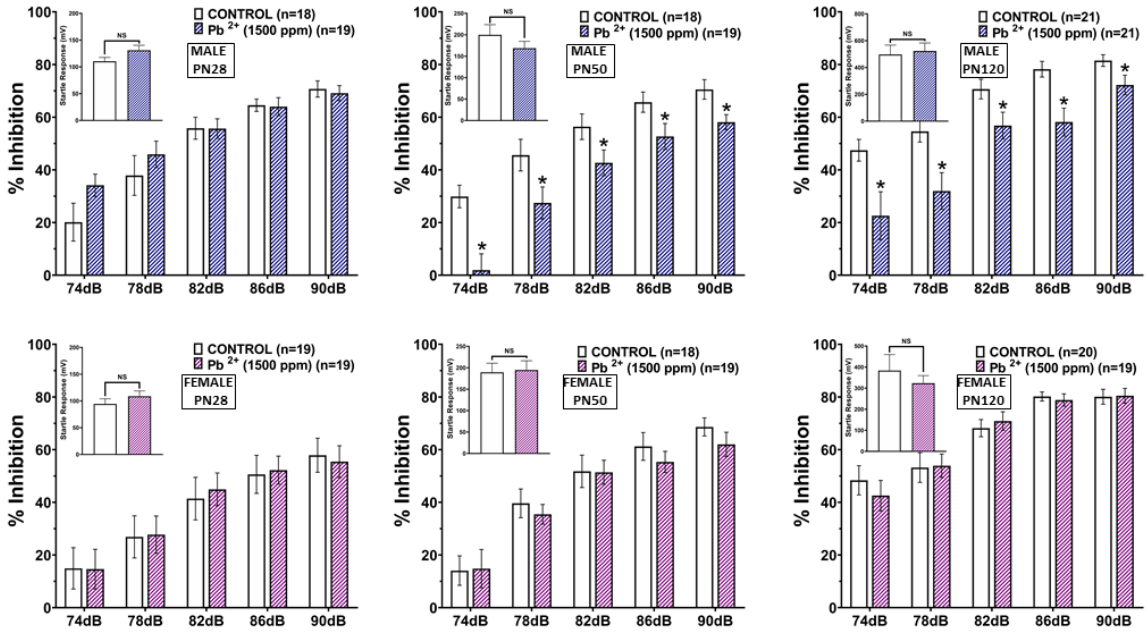

Figure 4. Prepulse inhibition in male and female rats chronically exposed to Pb^{2+}. The results show no effect of Pb^{2+} exposure at PN28 but marked inhibition of PPI in male rats at PN50 and PN120. No effect of Pb^{2+} exposure was found in female rats at any age. Insert graphs in each panel are startle response at 120 dB. No effect on startle response was observed in Pb^{2+}-exposed male or female rats relative to controls at any age. Thus, CELLE does not alter the sensitivity of the animal to a startle. However, CELLE produces a significant deficit on PPI in male rats relative to controls (*$p<0.05$). Data are expressed as mean ± sem. n=number of litters (one male and female animal per litter).

AGE	PN28		PN50		PN120	
SEX	Males	Females	Males	Females	Males	Females
Control	≤1.9 n=18	≤1.9 n=16	≤1.9 n=17	≤1.9 n=15	≤1.9 n=17	≤1.9 n=15
1500ppm PbAc	21.1 ± 0.9 n=18	20.9 ± 1.1 n=16	20.2 ± 1.1 n=17	22.1 ± 1.3 n=20	19.6 ± 1.3 n=17	24.3 ± 2.2 n=14
p-value	≤0.0001	≤0.0001	≤0.0001	≤0.0001	≤0.0001	≤0.0001

Table 1: Blood Pb^{2+} levels (µg/dL) in male and female rats contributing to data represented in Figure 9. Each value is the mean ± sem. n= number of litters (one male and female animal per litter).

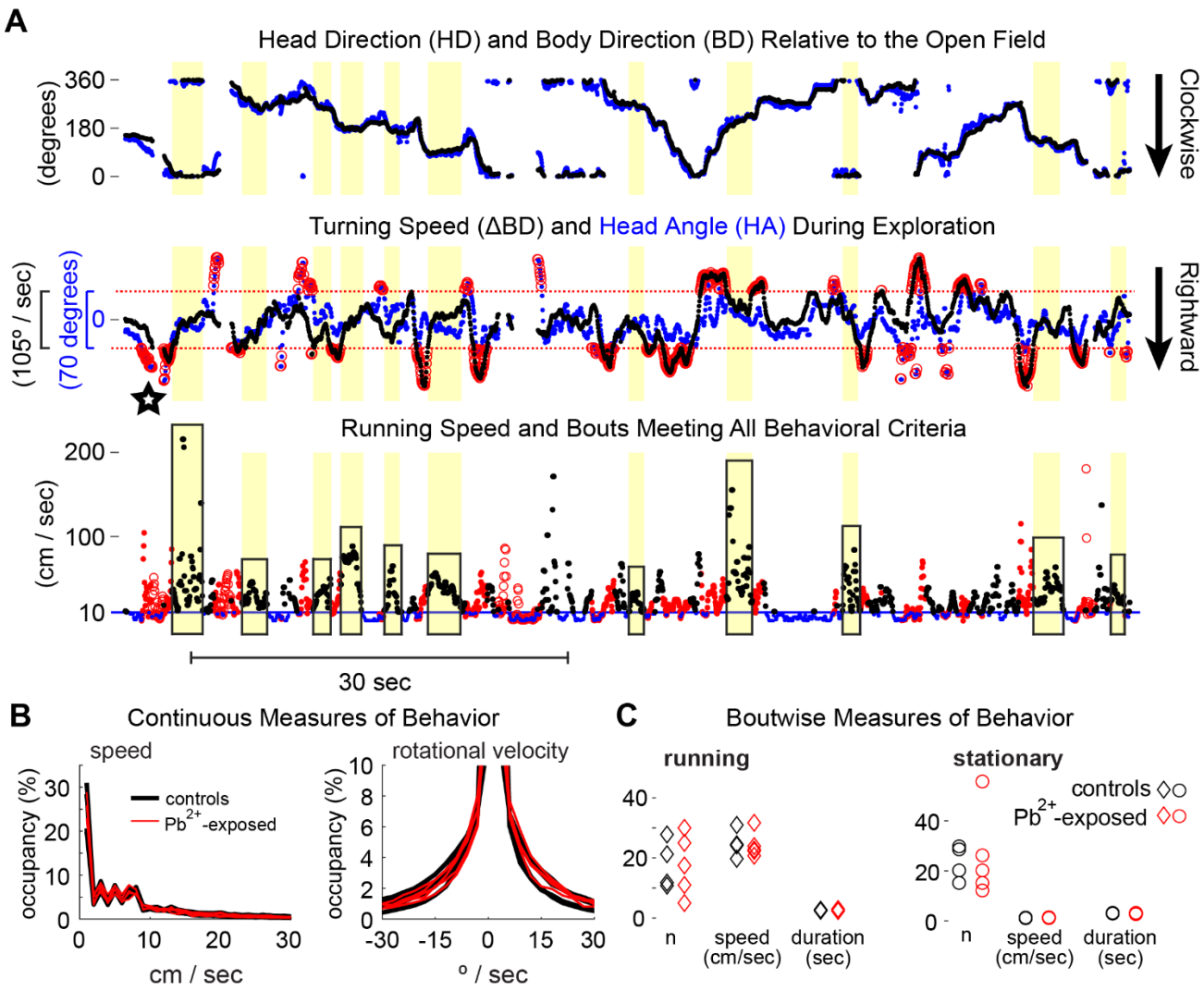

Supplemental Figure 1. Precise delineation of stationary and running bouts. A. Head and body direction (**top**) were used to derive rotational velocity and head angle (**middle**), which in turn were used to identify bouts of running (boxed at **bottom**) while excluding rotational and reorienting behaviors (red points and circles). **B.** Speed occupancy (**left**) and rotational velocity (**right**) measured throughout behavioral sessions did not differ between control and Pb^{2+}-exposed rats, nor did bout-wise behavioral measures (**C**) of running (**left**) and stationary bouts (**right**), including the numbers of bouts, median movement speeds, and bout durations.

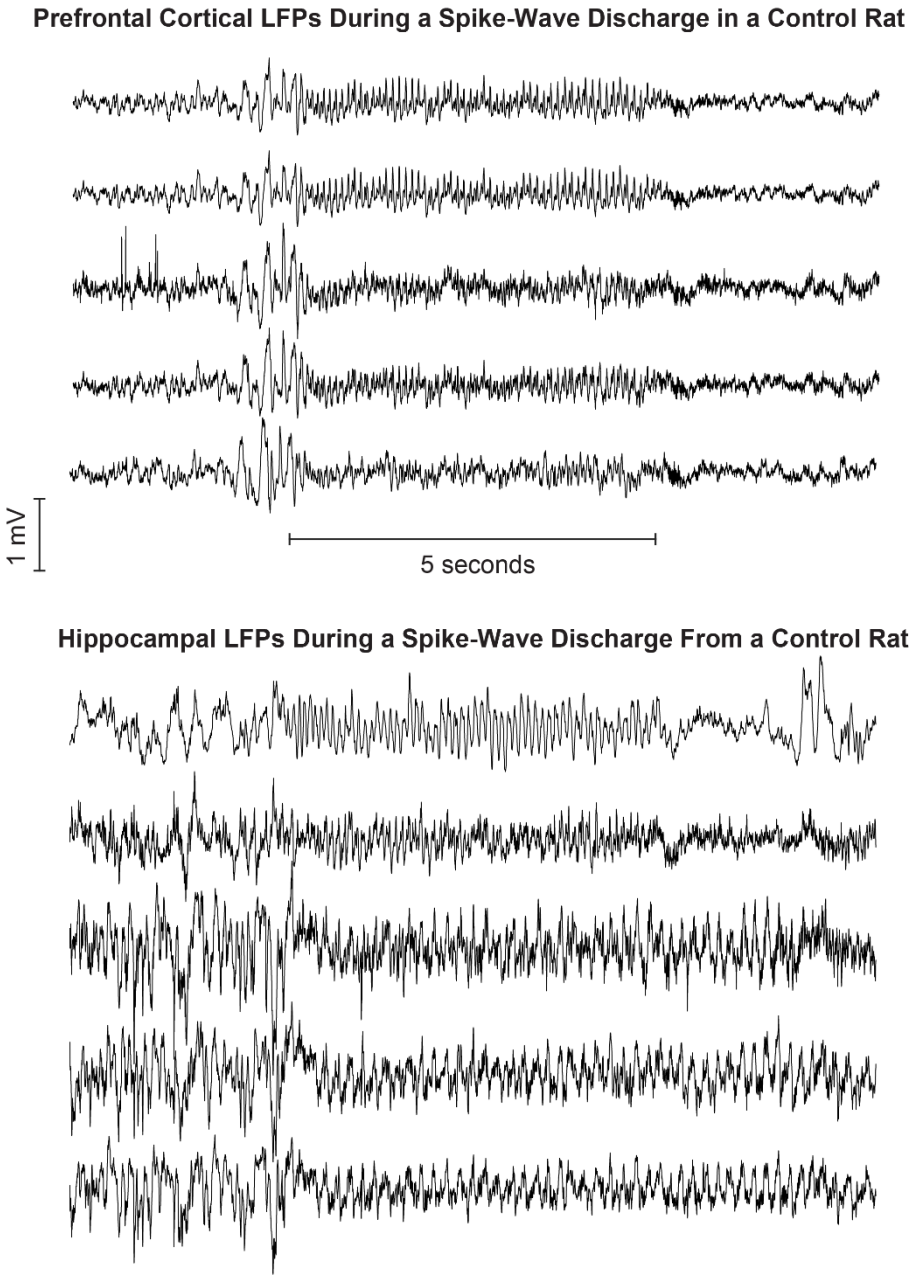

Supplemental Figure 2. Spike-wave discharge in a normal rat. An example of a spike wave discharge recorded in a control animal simultaneously at several prefrontal cortical sites (above) and hippocampal sites (below). Note, hippocampal sites showed considerable variability in terms of the LFP waveform during the seizure and in the continuation of theta oscillations follow seizure offset.

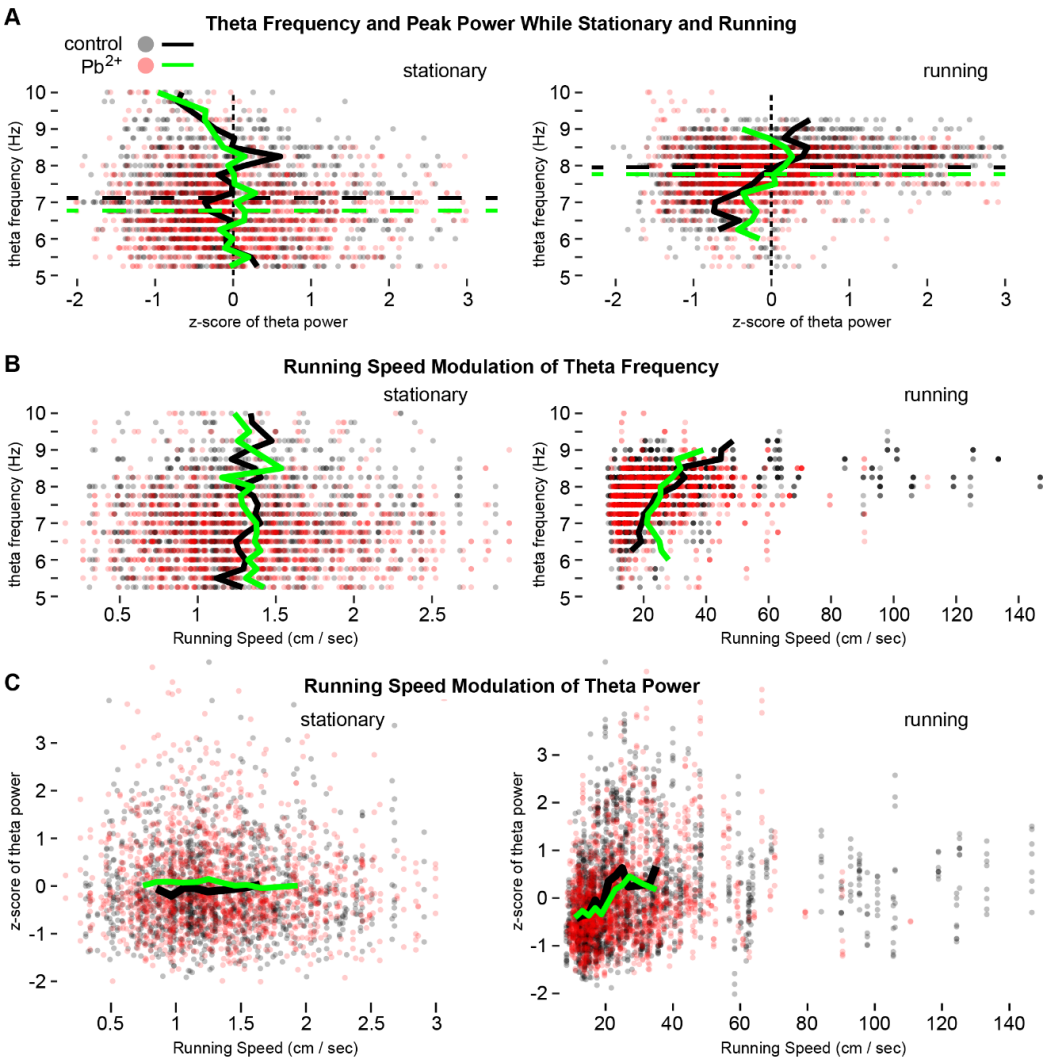

Supplemental Figure 3. Pb^{2+} exposure reduces theta frequency and disrupts running speed modulation. A. Scatter plots of theta power and frequency taken from the power spectral density for each recorded channel during each bout of stationary (**left**) and running behaviors (**right**) for all rats. Black and green lines indicate means for control and Pb^{2+}-exposed rats, respectively. Dashed lines indicate the mean theta frequencies for each group. **B.** Running speed modulation of theta frequency. **C.** Running speed modulation of theta power.

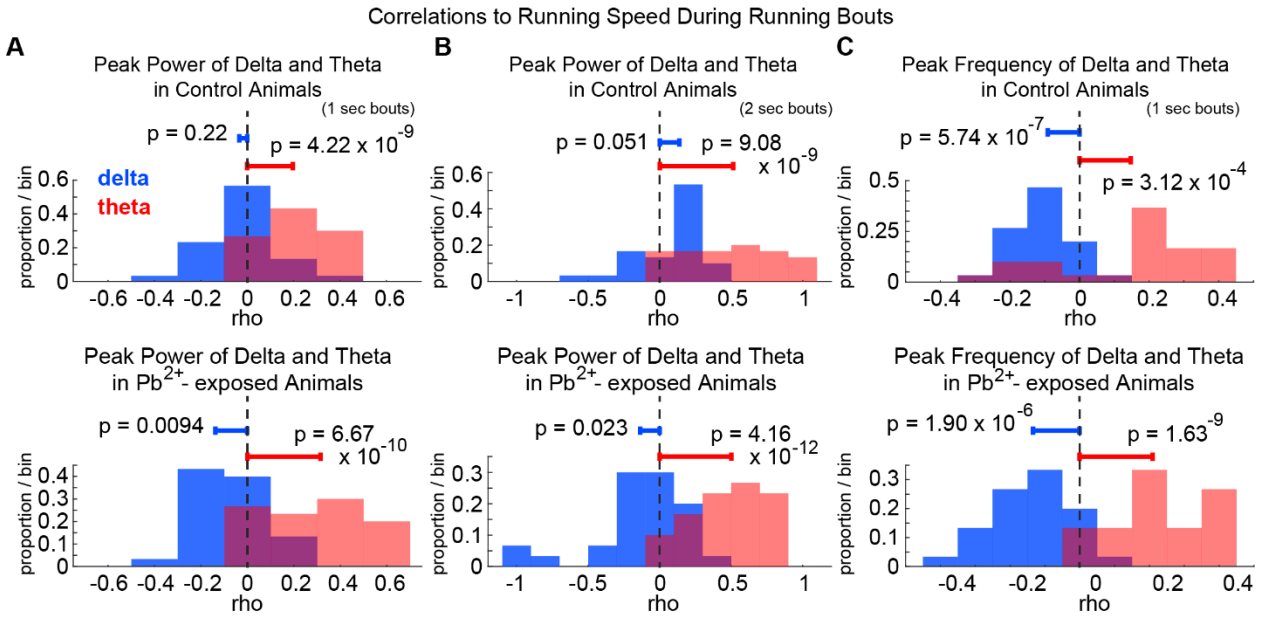

Supplemental Figure 4. Running speed modulation of theta power is elevated in Pb^{2+}-exposed animals. A. Distributions of correlation coefficients between delta (blue) and theta (red) power estimates and running speed. Individual correlations were calculated across running bouts (1 sec) for each recorded channel from control rats (**top**) and Pb^{2+}-exposed rats (**bottom**). **B.** As in A, for two second running bouts. **C.** As in A, but comparing correlations of delta and theta peak frequencies to running speed.

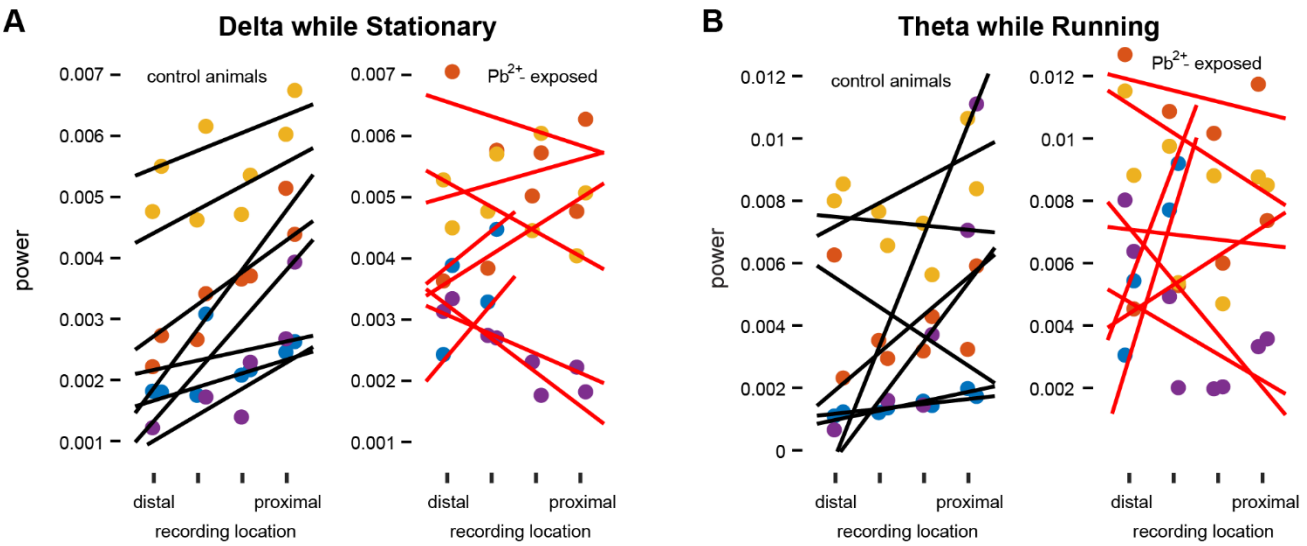

820

821 **Supplemental Figure 5. Proximal-distal gradient of delta and theta power in hippocampus. A.**
822 An apparent proximal-distal gradient in delta power across probe shanks in stationary control
823 animals (**left**), was absent in Pb^{2+}-exposed animals (**right**). Black and red lines in A and B reflect
824 the best fits to power estimates along the dorsal and ventral rows of four tetrodes (across shanks)
825 for each rat. **B.** Theta power at sites along the proximal-distal axis in control and Pb^{2+}-exposed
826 animals during running bouts.
827
828

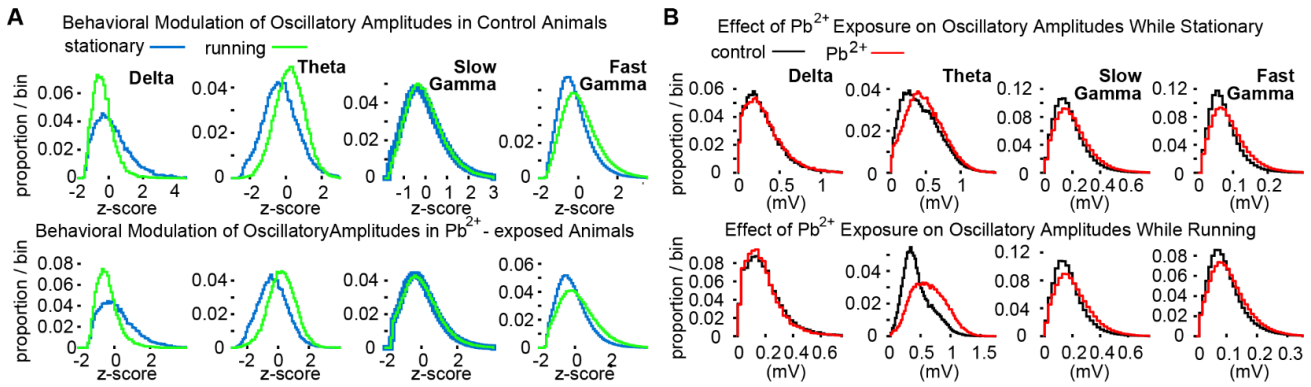

Supplemental Figure 6. Pb^{2+} exposure amplifies theta and gamma-frequency synchrony. A. Distributions of normalized cycle amplitudes for delta, theta, and gamma frequency bands during stationary (blue) and running bouts (green) in control (**top**) and Pb^{2+}-exposed animals (**bottom**). **B.** Distributions of unnormalized cycle amplitudes for each frequency band during stationary (**top**) and running bouts (**bottom**) in control (black) and Pb^{2+}-exposed animals (red).